

Submitted: Astrophysical Journal, September 2008

The Cepheid Period-Luminosity Relation at Mid-Infrared Wavelengths: II. Second-Epoch LMC Data

Barry F. Madore, Wendy L. Freedman, Jane Rigby
S. E. Persson, Laura Sturch & Violet Mager

*Observatories of the Carnegie Institution of Washington
813 Santa Barbara St., Pasadena, CA 91101*

wendy@ociw.edu, barry@ociw.edu, jrigby@ociw.edu, persson@ociw.edu,
lsturch@ociw.edu, vmager@ociw.edu

ABSTRACT

We present revised and improved mid-infrared Period-Luminosity (PL) relations for Large Magellanic Cloud (LMC) Cepheids based on double-epoch data of 70 Cepheids observed by *Spitzer* at 3.6, 4.5, 5.8 and 8.0 μm . The observed scatter at all wavelengths is found to decrease from ± 0.17 mag to ± 0.14 mag, which is fully consistent with the prediction that the total scatter is made up of roughly equal contributions from random sampling of the light curve and nearly-uniform samplings of stars across the instability strip. It is calculated that the Cepheids in this sample have a full amplitude of about 0.4 mag and that their fully-sampled, time-averaged magnitudes should eventually reveal mid-infrared PL relations that each have intrinsic scatter at most at the ± 0.12 mag level, and as low as ± 0.08 mag after correcting for the tilt of the LMC.

1. INTRODUCTION

In an earlier paper (Freedman et al. 2008, hereafter Paper I) we presented a preliminary calibration of the mid-infrared LMC Cepheid Period-Luminosity (PL) relations at 3.6, 4.5, 5.8 and 8.0 μm followed by an analysis of the wavelength dependence of the slopes and scatter in those relations. Those observations were derived from data serendipitously obtained by *Spitzer* during the course of the *Surveying the Agents of a Galaxy's Evolution* (SAGE) Project (Meixner et al. 2006a). The main conclusion was that even single-phase data (for known Cepheids with published periods) provided PL relations that had a mean scatter of only

about ± 0.17 mag, largely independent of wavelength. A plausible case was made that about half of the scatter was due to the random-phase nature of single observations (sampling light curves with a full amplitude of 0.3-0.4 mag), and that the other half of the scatter was being contributed by the intrinsic width of the instability strip. The latter was then self-consistently estimated to have an edge-to-edge width of 0.3-0.4 mag. Here we consider the effects of doubling the number of observations of the same (fixed size) sample of 70 long-period LMC Cepheids as were examined in Paper I.

The second (and last) installment of the combined and revised catalog¹ of point sources in the LMC has been released by the SAGE team. We have taken 4-band photometry from this catalog for epochs 1 and 2; the epoch 1 photometry was replaced by the SAGE team for consistency. This provides us with 560 individual observations of 70 Cepheids spread over 4 wavelengths and separated in time by about 7 months. The quoted precision of the individual data points varies systematically with period/magnitude, ranging from ± 0.01 mag for the brightest (longest-period) Cepheids at about 80 days, up to ± 0.10 mag for the faintest (short-period) Cepheids in our sample at about 6 days. The individual observations for both epochs are listed in Table 1, revising and updating our earlier tabulation in Freedman et al. (2008).

Our sample is based on the Persson et al. (2004) subset of well-observed LMC Cepheids selected to be uncrowded. Significantly larger samples (200 to nearly 600 stars, depending on wavelength) have been studied by Ngeow & Kanbur (2008). Their analysis results in some very different conclusions from ours. We comment briefly on these differences and explore their probable origin at the end of Sections 2 and 3.

2. IRAC Mid-Infrared Period-Luminosity Relations

The four mid-IR period-luminosity relations, presenting all 560 random-phase observations of the 70 Cepheids, are given in Figures 1 and 2. Details of the SAGE observations are given in Paper I; here we simply note that for some of the Cepheids the data for the reprocessed photometry differs slightly from the previous release used in Paper I. In this paper we use the most recently processed photometry for both epochs. The solid line gives a least-squares fit to the plotted data. The dashed lines mark the two-sigma limits on the scatter in each of the PL relations taken from Paper I. Despite the factor-of-two increase in the number of observations it is interesting to note that virtually all of the new data points fall within the previous limits. This was to be expected if the observed range of the

¹Available from IRSA at <http://irsa.ipac.caltech.edu/data/SPITZER/SAGE/>

distribution is being defined by random sampling of finite-amplitude light curves. If the scatter were instead dominated by random errors in the photometry alone, the range would increase with sample size; it does not. We can then with some confidence go on to interpret the scatter physically.

Averaging the two-epoch photometry for individual Cepheids significantly decreases the scatter about the mean PL relation. This is because averaging brings us closer to the time-averaged mean magnitude of the individual Cepheids (by damping out the phase-induced excursions.)

How much of the total scatter is due to the random sampling of the light curves, and how much is due to the intrinsic width of the Cepheid instability strip, projected into the period-luminosity plane? In Paper I we suggested that the split was 50:50. We can now quantitatively test that prediction.

2.1. Period-Luminosity Fits

Weighted, least-squares, linear fits to each of the four mid-IR data sets are given in Section 3. The slopes, zero points, respective errors and *rms* scatter, listed for each bandpass, are consistent with our previous results from Paper I. The slopes at each wavelength all have values of around -3.4, with a slight trend of increasingly negative values towards longer wavelengths. The scatter around each of the fits is relatively constant at ± 0.16 - 0.17 mag; and from filter to filter the scatter of individual data points is highly correlated (see Figures 3-5 and discussion below).

2.2. Correlations in the Scatter

In Figure 5 we show the highly correlated nature of the magnitude differences in a given band plotted against the magnitude differences for the same stars, but at the other wavelengths. Clearly the observed differences are not random noise, but rather due to the physically correlated changes generated by light variation of the Cepheids themselves. Since there appears to be no significant deviation from a one-to-one correspondence in these variations, this is consistent with the dominant contributor in each of these bands being due to radius variations, as expected at these long wavelengths (Madore & Freedman 1991).

If the magnitude differences in the two observations are purely a result of changes intrinsic to the Cepheid during its cycle then the distribution of those differences should be consistent with our expected mid-infrared light curve and that distribution should reach a

maximum at the full amplitude. Consulting the lower right panel in Figure 8 of Madore & Freedman (2005) which shows the marginalized distribution of amplitudes for a two-epoch, random sampling of a Cepheid light curves, shows that the expected distribution function should be triangular in form with its peak at zero difference between consecutive observations and its minimum at a value corresponding to (the unlikely, two-point, chance-sampling of) the full amplitude of the lightcurve. Examination of Figure 6 shows that the observed distributions of differences (upper histograms) correspond to this prediction and that the most probable amplitude for these Cepheids at all wavelengths is 0.4-0.5 mag. The lower portion of the main plot showing each of the individual differences (with symbols encoded by wavelength) indicates that there may be a slow decline of mean/maximum amplitude with decreasing period from a maximum amplitude of 0.5 mag around 40 days, falling to a maximum amplitude of 0.3 mag below 10 days.

We are now in a position to test the assumption made in Paper I that the measured variance in the single-phase PL relation is shared equally between the random sampling of the instability strip and the phase sampling of the individual light curve where the width of the instability strip (0.40 mag) contributes a scatter of ± 0.12 mag and the amplitudes of the individual Cepheids (also 0.4 mag peak-to-peak) contribute another ± 0.12 mag of scatter.

That is, if σ_1 is the scatter around the PL relation measured for the single-epoch data, and σ_2 is the scatter measured for the time-averaged two-epoch data then:

$$\begin{aligned}\sigma_1^2 &= \sigma_{strip}^2 + \sigma_{cepheid}^2 \\ \sigma_2^2 &= \sigma_{strip}^2 + \sigma_{cepheid}^2/2\end{aligned}$$

Thus

$$\sigma_{cepheid}^2 = 2(\sigma_1^2 - \sigma_2^2)$$

and

$$\sigma_{strip}^2 = 2\sigma_2^2 - \sigma_1^2$$

Converting observed scatter to intrinsic width (i.e., $\sigma_{strip} \times \sqrt{N}$) gives strip widths of 0.36, 0.37, 0.36 and 0.37 mag at 3.6, 4.5, 5.8 and 8.0 μm , respectively, and average Cepheid amplitudes of 0.43, 0.45, 0.43 and 0.43 mag in those same respective bandpasses. These amplitudes correspond well to the independently-estimated amplitudes derived from the magnitude-difference histograms discussed above.

What this means in practice is that, given the choice between observing more Cepheids or observing more phase points for the same set of Cepheids in order to reduce the error on the distance modulus, increasing the number of observations per Cepheid is initially

more effective given the larger amplitude of the stars compared to the intrinsic width of the instability strip. The advantage of numbers of observations over numbers of stars is about 3:2 in the variance, which scales inversely with N .

The short-wavelength residuals reported by Ngeow & Kanbur (2008) based on a completely different and considerably larger sample of 200 to 600 LMC Cepheids (depending on the wavelength), are significantly smaller than the values given here. For instance, they give (their Tables 2 & 4) a scatter about the mean of ± 0.10 mag for the 3.6 and $4.5\mu\text{m}$ PL relations. Following the line of argument given above such small scatter (if real) would reduce both the amplitudes and the width of the instability strip to implausibly small values. Our data do not support those conclusions. It is possible that the procedures used by Ngeow & Kanbur in an attempt to remove outliers resulted in this remarkably low dispersion.

3. Absolute Calibration

In keeping with Paper I, we adopt a true distance to the Large Magellanic Cloud of $(m-M)_o = 18.50$ mag and a mean reddening to the Cepheids of $E(B-V) = 0.10$ mag (Freedman *et al.*, 2001). Applying this correction for the true distance modulus and applying extinction corrections (0.04 to 0.01 mag), we derive the following updated absolute calibrations for the Cepheid Period-Luminosity relations at mid-infrared wavelengths:

$$\langle M \rangle_{3.6} = -3.40(\log(P) - 1.0) [\pm 0.02] - 5.81 [\pm 0.03] \quad \sigma_{3.6} = \pm 0.135$$

$$\langle M \rangle_{4.5} = -3.35(\log(P) - 1.0) [\pm 0.02] - 5.76 [\pm 0.03] \quad \sigma_{4.5} = \pm 0.141$$

$$\langle M \rangle_{5.8} = -3.44(\log(P) - 1.0) [\pm 0.03] - 5.81 [\pm 0.04] \quad \sigma_{5.8} = \pm 0.137$$

$$\langle M \rangle_{8.0} = -3.49(\log(P) - 1.0) [\pm 0.03] - 5.81 [\pm 0.04] \quad \sigma_{8.0} = \pm 0.139$$

The last entry in each line is the scatter measured about the preceding regression line. The above-quoted slopes and their generally monotonic increase with wavelength (consistent with and confirming Figure 4, Paper I) are in conflict with the generally lower values and especially the puzzling reversal of the slopes with wavelength given by Ngeow & Kanbur (2008). We speculate that their increased sample size brings with it crowding and other photometric errors that affect their solutions. Certainly the dramatic increase in dispersion

around their solutions at longer wavelengths must be the result of photometric uncertainties and not due to (or expected from) physical processes intrinsic to the Cepheids themselves.

However, we note that there is still two additional sources of identifiable variance in these solutions: (1) back-to-front geometric effects due to the tilt of the LMC and (2) a spread of metallicity amongst the LMC Cepheids themselves. The analysis of Persson et al. (2004), given in their Table 6, clearly indicates that tilt contributes about ± 0.08 mag of scatter to all solutions using this Cepheid sample. Removing that geometric term would suggest that the underlying (time-averaged) mid-infrared PL relations have an intrinsic scatter of ± 0.08 mag. The compilation of measured atmospheric metallicities of individual LMC Cepheids by Romaniello et al. (2008) shows a spread of 0.5 dex in $[\text{Fe}/\text{H}]$. Any impact of this dispersion of metallicity on the mid-infrared magnitudes of these LMC Cepheids must be fully contained within the ± 0.08 mag of residual scatter. However this scatter cannot be totally due to metallicity since there must ultimately be contributions due to mean-radius and mean-temperature variations of the Cepheids across the instability strip. Each of these second-order effects and any others that have not yet been explicitly considered (residual crowding effects and unresolved binary stars in the sample, for example) all must be contained in the residual scatter of ± 0.08 mag.

4. Conclusions and Future Prospects

The total magnitude width of the LMC Cepheid instability strip at mid-infrared wavelengths is found to be 0.36 mag (uncorrected for the LMC tilt). This translates into an *rms* scatter of ± 0.11 mag around any one of the four time-averaged, mid-infrared PL relations. In order to obtain a distance modulus statistically good to ± 0.01 mag would require a sample of approximately 100 Cepheids. We further calculate that the average mid-IR amplitude of Cepheids in our sample is (peak-to-peak) 0.43 mag. To obtain time-averaged mean magnitudes for individual Cepheids good to ± 0.02 mag would then require on the order of 36 randomly-phased observations.

Testing the mid-infrared PL relations for their sensitivity to metallicity, and providing an absolute calibration that is independent of the LMC distance scale are the obvious next steps in this process. However, Spitzer alone is certainly capable of detecting Cepheids out to 1-2 Mpc using reasonable (1-2 hour) integration times, but crowding from AGB and extended-AGB stars is likely to be the real limiting factor. Applications to galaxies appreciably beyond the Local Group and their use in shoring up the extragalactic distance scale must await JWST.

References

- Freedman, W. L., *et al.* 2001, ApJ, 553, 47
- Freedman, W. L., Madore, B.F., Rigby, J., Persson, S.E., & Sturch, L. 2008, ApJ, 679, 71
- Madore, B. F., & Freedman, W. L. 2005, PASP, 103, 933
- Madore, B. F., & Freedman, W. L. 2005, ApJ, 630, 1054
- Ngeow, C., & Kanbur, S.M. 2008, ApJ, 679, 76
- Meixner, M., *et al.* 2006, AJ, 132, 2268
- Persson, S.E., Madore, B.F., Krzeminski, W., Freedman, W.L., Roth, M. & Murphy, D.C., AJ, 128, 2239
- Romaniello et al., 2008, A&A, 488, 731
- Schaltenbrand, R. & Tammann, G.A., 1970, A&A, 7, 289

Figure Captions

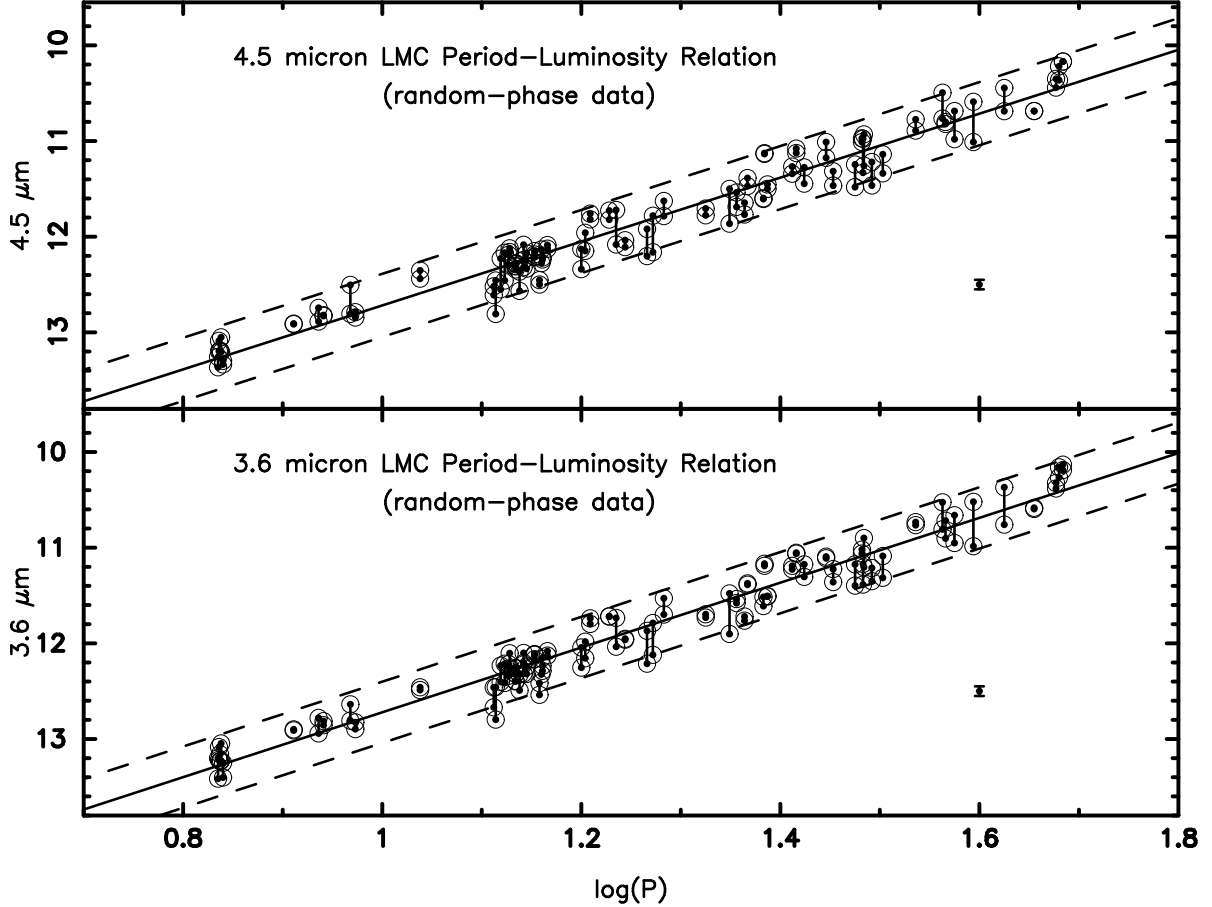


Fig. 1 – Random-phase (3.6 and 4.5 μm) IRAC Period-Luminosity relations for LMC Cepheids plotted over the $\log(P)$ range 0.7 to 1.8. Observations of the same star seen at different epochs are joined by solid vertical lines. The solid line is a weighted least-squares fit to the data. The broken lines represent $\pm 2\sigma$ (typically ± 0.33 mag) bounds on the instability strip taken from the single-phase data fits, consistent with Paper I. Note that virtually all of the new data points fall within the old boundaries: despite a factor of two increase in numbers of data points the range does not appear to increase. The sizes of the plotted symbols are comparable to the typical photometric error on a mid-range Cepheid, i.e., ± 0.05 mag at $\log(P) = 1.3$. A magnitude error of ± 0.05 mag is shown in the lower right corner of each figure; at the shortest periods the reported errors on a single observation can be as high as ± 0.10 mag.

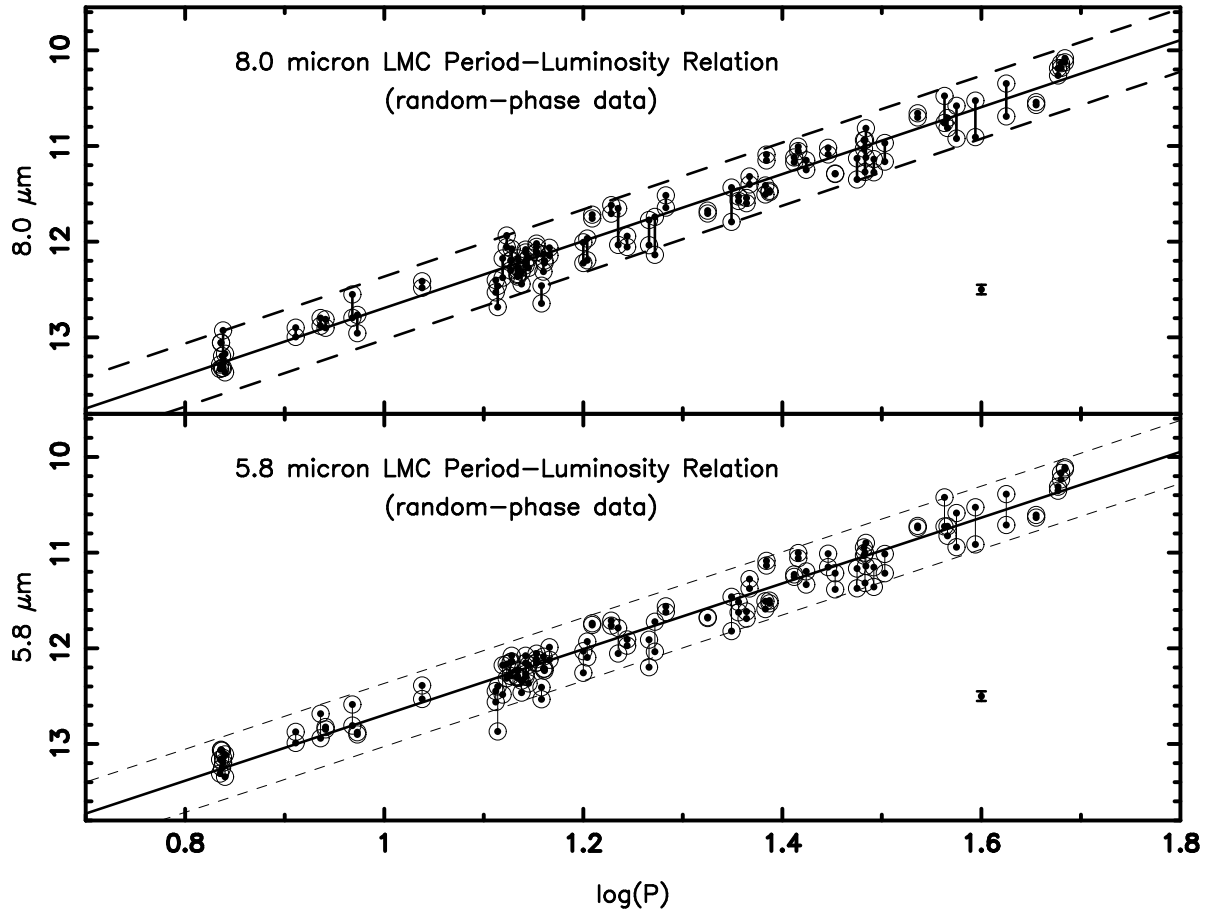


Fig. 2 – The same as Figure 1 except that the plots are for 5.8 and 8.0 μm IRAC data.

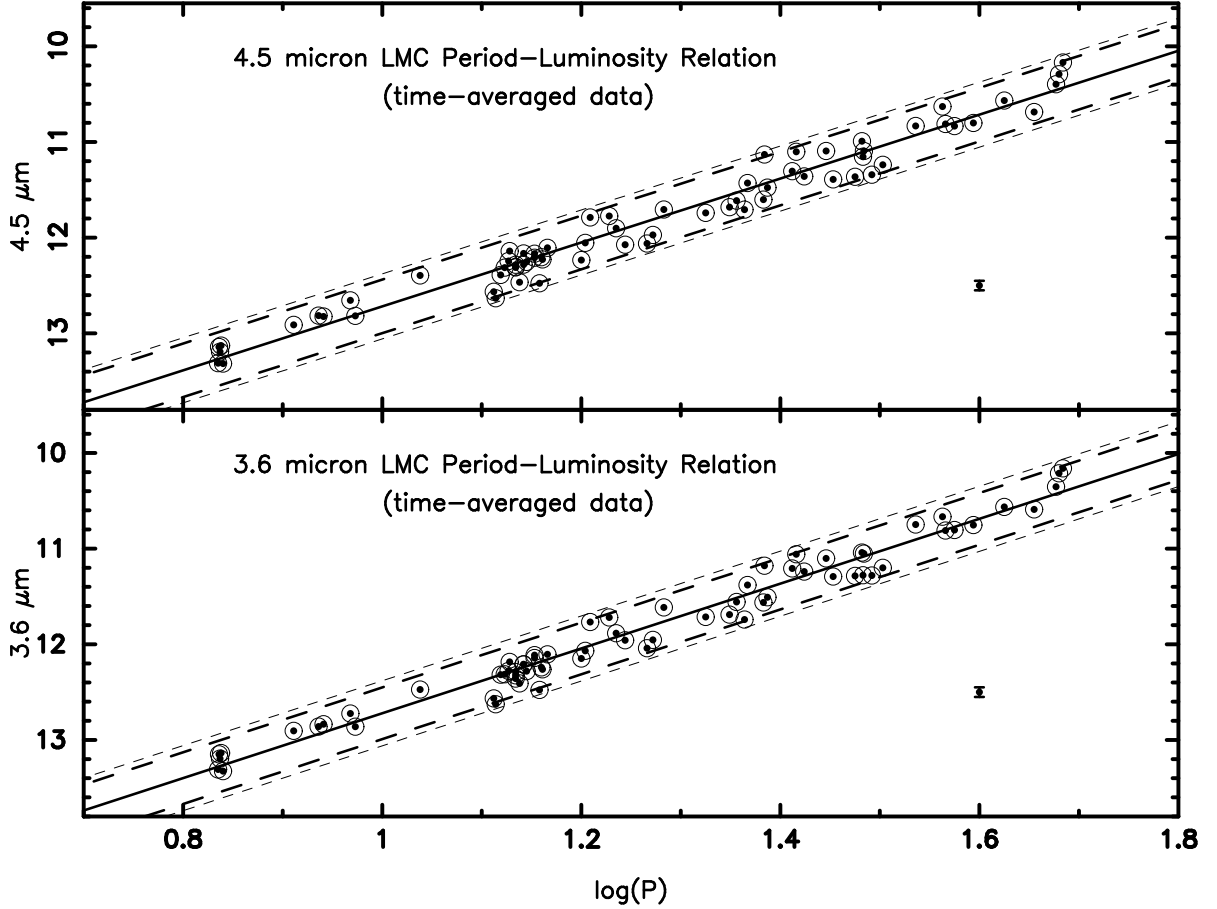


Fig. 3 – Time-Averaged (3.6 and $4.5\mu\text{m}$) IRAC Period-Luminosity relations for LMC Cepheids plotted over the $\log(P)$ range 0.7 to 1.8 . Only two epochs contributed to the average, nevertheless the scatter drops measurably from around ± 0.165 mag to about ± 0.140 mag (see Section 3). The solid line is a weighted least-squares fit to the data. The thick broken lines are the $\pm 2\sigma$ (typically ± 0.28 mag) bounds on the instability strip taken from fits to the plotted time-averaged datasets. The thin dashed lines are the two-sigma bounds on the instability strip from Figures 1 & 2. The shrinkage between the two limits is significant and is interpreted in the text. The sizes of the plotted symbols are comparable to the typical photometric error on a mid-range Cepheid, i.e., ± 0.05 mag at $\log(P) = 1.3$. A magnitude error of ± 0.05 mag is shown in the lower right corner of each figure; at the shortest periods the reported errors on a single observation can be as high as ± 0.10 mag.

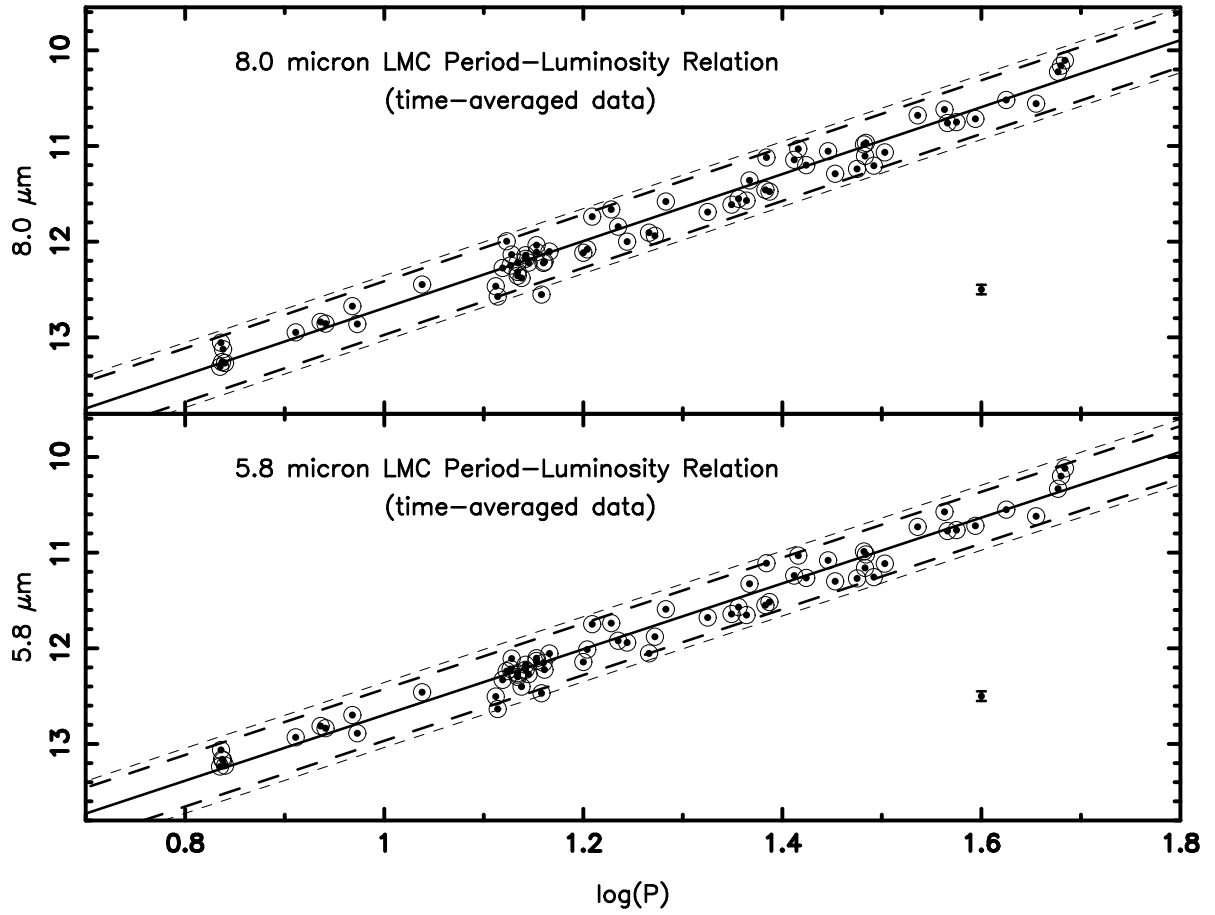


Fig. 4 – Time-averaged (5.8 and 8.0 μm) IRAC Period-Luminosity relations for LMC Cepheids plotted over the log(P) range 0.7 to 1.8; otherwise see caption to Figure 3.

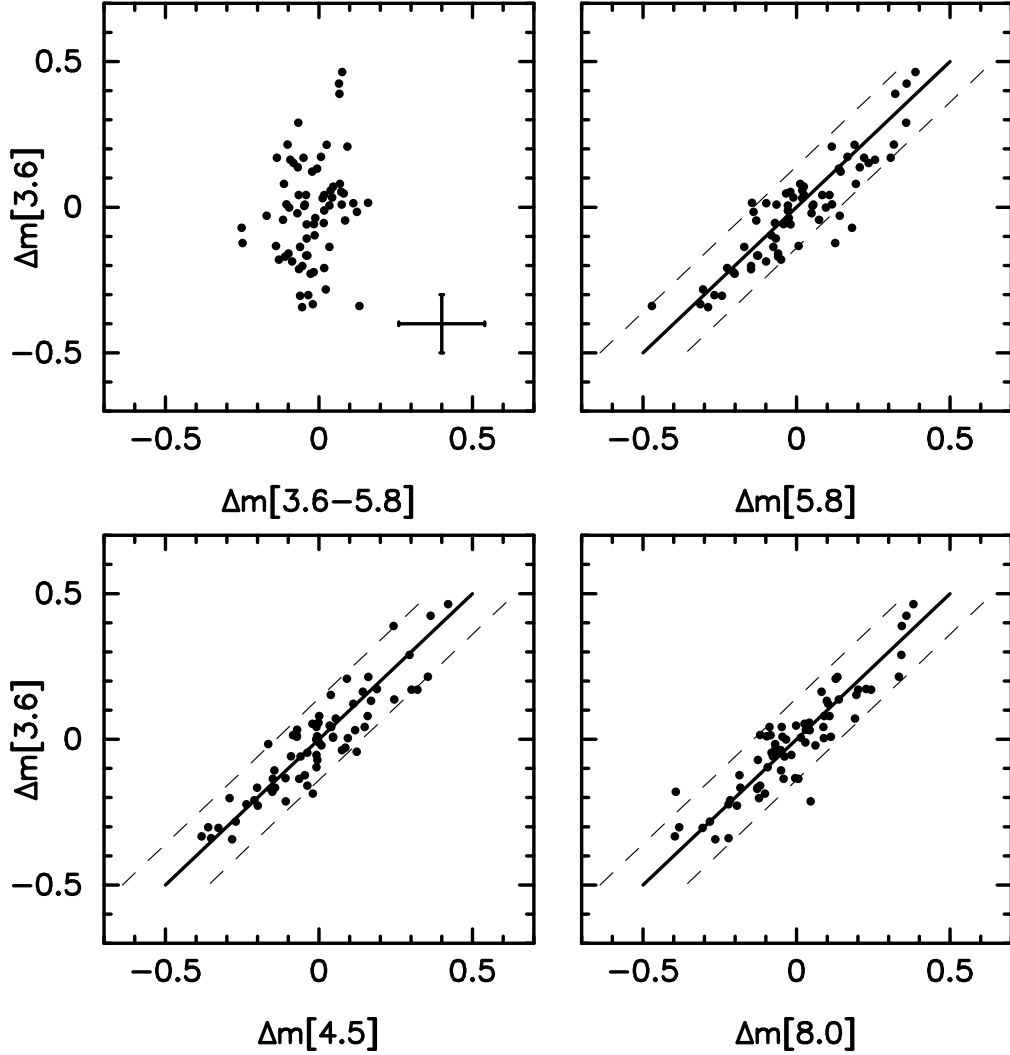


Fig. 5 – Correlated residuals from the PL and (upper left panel) PC fits. Deviations of individual phase points from the mean PL regression are shown to be highly correlated across the respective bandpasses. A unit-slope line is shown for reference, and scatter around that line is seen to be consistent with the photometric errors (typically ± 0.05 mag) quoted for the individual observations. Maximum (correlated) excursions have an upper bound of ± 0.4 mag which is probably representative of the full amplitude of Cepheids at these wavelengths. The upper left panel is illustrative of the lack of any significant correlation between magnitude and color residuals, primarily because there is no statistically significant change (with phase) in the colors of these Cepheids at mid-IR wavelengths. A typical (two-sigma) error bar is shown in the lower righthand corner of this plot: the change in magnitude for a given star is statistically significant, the change in color is not.

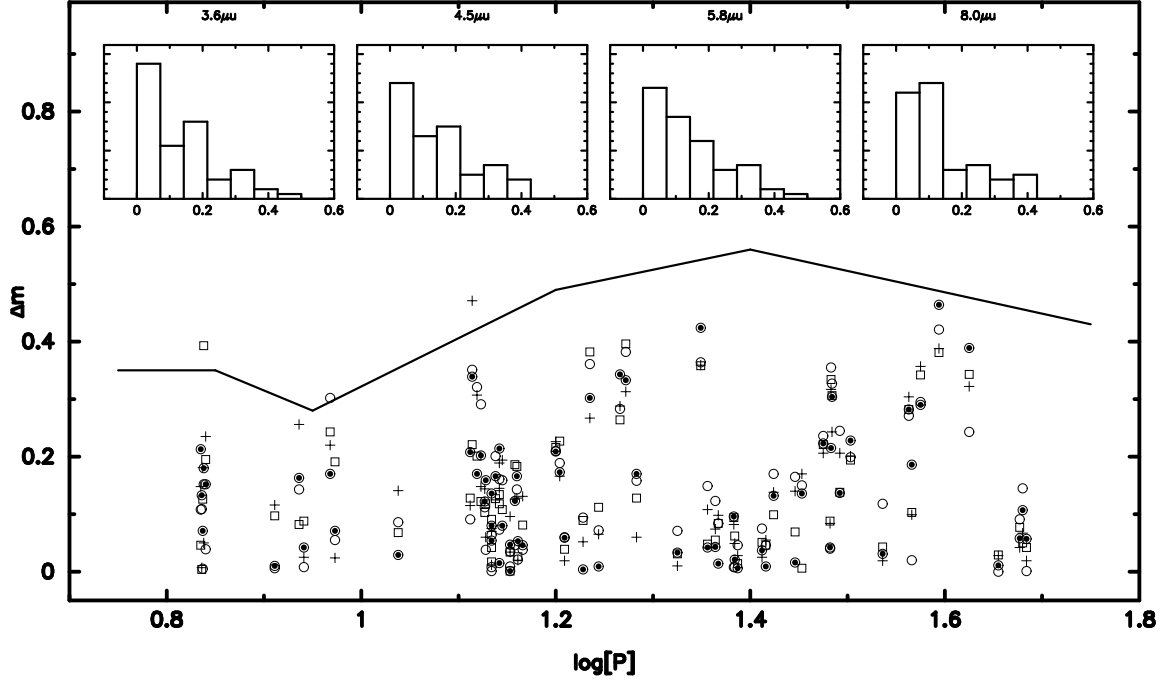


Fig. 6 – The absolute values of magnitude differences between the two epochs for the same star as a function of the period. Filled circles are 3.6 μm amplitudes, open circles are 4.5 μm data. Crosses and squares are magnitude differences for 6.8 and 8.0 μm data, respectively. Note the possible increase in the maximum difference as a function period, consistent with the scaled upper envelope to the optical Period-Amplitude relation from Schaltenbrand & Tammann (1970), shown the series of broken straight lines. The histograms in the upper part of the figure represent the marginalized and binned amplitude data for each of the four IRAC bands increasing in wavelength from left to right. As predicted from simulations (Madore & Freedman 2005), the form of the histograms should be triangular, as is observed; and the x intercept should be the full amplitude of the variable star. Each of the histograms is consistent with an amplitude of 0.4 mag, as independently calculated from the change in residuals around the PL relation, discussed in Section 2.2.

Table 1.

Cepheid	log(P) (days)	3.6 μ m (mag)	4.5 μ m (mag)	5.8 μ m (mag)	8.0 μ m (mag)
HV 872	1.475	11.174	11.245	11.167	11.129
		0.034	0.033	0.041	0.053
HV 872	1.475	11.397	11.481	11.373	11.350
		0.023	0.026	0.032	0.046
HV 873	1.536	10.764	10.891	10.740	10.701
		0.040	0.035	0.034	0.052
HV 873	1.536	10.733	10.773	10.721	10.658
		0.034	0.029	0.040	0.057
HV 875	1.482	11.062	11.011	11.030	11.027
		0.034	0.025	0.034	0.034
HV 875	1.482	11.020	10.971	10.946	10.939
		0.039	0.031	0.039	0.038
HV 876	1.356	11.579	11.687	11.624	11.527
		0.037	0.032	0.055	0.063
HV 876	1.356	11.537	11.538	11.516	11.575
		0.036	0.038	0.040	0.076
HV 877	1.655	10.584	10.687	10.606	10.571
		0.035	0.036	0.039	0.050
HV 877	1.655	10.595	10.687	10.634	10.542
		0.040	0.027	0.033	0.041
HV 878	1.367	11.387	11.387	11.277	11.318
		0.035	0.041	0.042	0.041
HV 878	1.367	11.373	11.471	11.375	11.402
		0.041	0.037	0.041	0.057
HV 879	1.566	10.718	10.801	10.725	10.708
		0.024	0.024	0.031	0.035
HV 879	1.566	10.904	10.821	10.824	10.811
		0.037	0.023	0.041	0.032
HV 882	1.503	11.087	11.139	11.014	10.969
		0.032	0.033	0.039	0.046

Table 1—Continued

Cepheid	log(P) (days)	3.6 μ m (mag)	4.5 μ m (mag)	5.8 μ m (mag)	8.0 μ m (mag)
HV 882	1.503	11.315	11.338	11.215	11.163
		0.053	0.034	0.036	0.050
HV 887	1.161	12.288	12.217	12.213	12.223
		0.052	0.074	0.065	0.056
HV 887	1.161	12.235	12.238	12.233	12.197
		0.039	0.042	0.050	0.057
HV 889	1.412	11.189	11.342	11.228	11.119
		0.042	0.060	0.050	0.053
HV 889	1.412	11.226	11.267	11.253	11.170
		0.058	0.043	0.048	0.053
HV 891	1.235	11.734	11.721	11.788	11.652
		0.041	0.042	0.049	0.059
HV 891	1.235	12.036	12.082	12.055	12.034
		0.051	0.047	0.070	0.058
HV 892	1.204	12.155	12.148	12.096	12.194
		0.048	0.038	0.042	0.066
HV 892	1.204	11.982	11.959	11.930	11.967
		0.038	0.033	0.051	0.056
HV 893	1.325	11.730	11.705	11.674	11.706
		0.051	0.037	0.065	0.053
HV 893	1.325	11.697	11.776	11.684	11.675
		0.044	0.042	0.056	0.051
HV 899	1.492	11.350	11.464	11.359	11.275
		0.032	0.039	0.049	0.049
HV 899	1.492	11.213	11.219	11.153	11.137
		0.035	0.042	0.068	0.041
HV 900	1.677	10.324	10.350	10.311	10.186
		0.027	0.029	0.034	0.044
HV 900	1.677	10.382	10.441	10.353	10.263
		0.023	0.029	0.028	0.043

Table 1—Continued

Cepheid	log(P) (days)	3.6 μ m (mag)	4.5 μ m (mag)	5.8 μ m (mag)	8.0 μ m (mag)
HV 901	1.266	11.870	11.919	11.910	11.773
		0.039	0.040	0.044	0.071
HV 901	1.266	12.213	12.202	12.198	12.037
		0.028	0.026	0.041	0.041
HV 904	1.483	11.386	11.331	11.318	11.271
		0.025	0.021	0.036	0.035
HV 904	1.483	11.171	10.976	11.001	10.937
		0.045	0.038	0.042	0.034
HV 909	1.575	10.951	10.981	10.943	10.922
		0.036	0.040	0.039	0.047
HV 909	1.575	10.661	10.686	10.586	10.580
		0.042	0.041	0.040	0.039
HV 914	0.838	13.046	13.052	13.145	12.927
		0.034	0.051	0.05	0.097
HV 914	0.838	13.226	13.204	13.195	13.320
		0.042	0.036	0.095	0.109
HV 971	0.968	12.808	12.806	12.808	12.795
		0.042	0.053	0.082	0.088
HV 971	0.968	12.638	12.504	12.588	12.552
		0.048	0.038	0.061	0.080
HV 932	1.123	12.213	12.167	12.165	11.935
		0.039	0.050	0.068	0.145
HV 932	1.123	12.415	12.458	12.313	12.057
		0.031	0.040	0.051	0.103
HV 953	1.680	10.159	10.219	10.167	10.135
		0.030	0.032	0.043	0.041
HV 953	1.680	10.266	10.364	10.234	10.185
		0.037	0.029	0.033	0.043
HV 997	1.119	12.403	12.550	12.484	12.376
		0.043	0.041	0.071	0.065

Table 1—Continued

Cepheid	log(P) (days)	3.6 μ m (mag)	4.5 μ m (mag)	5.8 μ m (mag)	8.0 μ m (mag)
HV 997	1.119	12.233	12.229	12.177	12.175
		0.032	0.038	0.053	0.059
HV 1002	1.484	10.900	10.930	10.898	10.814
		0.032	0.030	0.046	0.036
HV 1002	1.484	11.204	11.257	11.141	11.120
		0.037	0.041	0.037	0.046
HV 1003	1.387	11.511	11.499	11.502	11.483
		0.034	0.033	0.044	0.061
HV 1003	1.387	11.505	11.453	11.530	11.469
		0.043	0.033	0.042	0.051
HV 1005	1.272	11.787	11.780	11.722	11.741
		0.032	0.028	0.038	0.045
HV 1005	1.272	12.120	12.162	12.035	12.137
		0.035	0.049	0.057	0.073
HV 1006	1.153	12.113	12.205	12.152	12.020
		0.047	0.040	0.067	0.053
HV 1006	1.153	12.114	12.214	12.056	12.054
		0.052	0.059	0.066	0.058
HV 1013	1.383	11.515	11.598	11.508	11.412
		0.024	0.026	0.031	0.038
HV 1013	1.383	11.611	11.606	11.590	11.506
		0.041	0.033	0.051	0.057
HV 1019	1.134	12.262	12.279	12.240	12.348
		0.043	0.042	0.054	0.099
HV 1019	1.134	12.316	12.287	12.310	12.365
		0.038	0.031	0.052	0.064
HV 1023	1.424	11.306	11.445	11.334	11.249
		0.035	0.031	0.037	0.044
HV 1023	1.424	11.174	11.275	11.196	11.150
		0.027	0.036	0.041	0.050

Table 1—Continued

Cepheid	log(P) (days)	3.6 μ m (mag)	4.5 μ m (mag)	5.8 μ m (mag)	8.0 μ m (mag)
HV 2244	1.145	12.321	12.333	12.367	12.273
		0.052	0.043	0.065	0.064
HV 2244	1.145	12.241	12.174	12.173	12.165
		0.045	0.031	0.058	0.062
HV 2251	1.446	11.094	11.011	11.011	11.019
		0.027	0.045	0.037	0.042
HV 2251	1.446	11.110	11.176	11.151	11.088
		0.031	0.036	0.032	0.030
HV 2257	1.594	10.985	11.011	10.914	10.907
		0.038	0.041	0.039	0.048
HV 2257	1.594	10.521	10.590	10.526	10.526
		0.044	0.031	0.036	0.046
HV 2260	1.114	12.458	12.457	12.399	12.463
		0.041	0.035	0.045	0.051
HV 2260	1.114	12.797	12.808	12.870	12.684
		0.065	0.039	0.080	0.090
HV 2270	1.134	12.398	12.309	12.305	12.265
		0.047	0.034	0.063	0.068
HV 2270	1.134	12.318	12.308	12.293	12.174
		0.054	0.029	0.055	0.058
HV 2282	1.166	12.082	12.087	11.989	12.063
		0.066	0.042	0.051	0.068
HV 2282	1.166	12.128	12.125	12.120	12.144
		0.051	0.041	0.059	0.069
HV 2291	1.349	11.902	11.863	11.821	11.792
		0.040	0.046	0.066	0.052
HV 2291	1.349	11.478	11.499	11.462	11.434
		0.035	0.041	0.045	0.037
HV 2294	1.563	10.526	10.494	10.422	10.477
		0.047	0.035	0.043	0.047

Table 1—Continued

Cepheid	log(P) (days)	3.6 μ m (mag)	4.5 μ m (mag)	5.8 μ m (mag)	8.0 μ m (mag)
HV 2294	1.563	10.808	10.765	10.726	10.759
		0.035	0.029	0.044	0.036
HV 2324	1.160	12.159	12.133	12.087	12.130
		0.048	0.036	0.051	0.056
HV 2324	1.160	12.325	12.276	12.215	12.313
		0.046	0.040	0.056	0.077
HV 2337	0.837	13.159	13.189	13.251	13.195
		0.046	0.068	0.072	0.113
HV 2337	0.837	13.230	13.194	13.070	13.321
		0.051	0.070	0.088	0.129
HV 2338	1.625	10.759	10.688	10.711	10.690
		0.026	0.037	0.042	0.038
HV 2338	1.625	10.370	10.445	10.389	10.347
		0.028	0.020	0.031	0.031
HV 2339	1.142	12.315	12.245	12.267	12.247
		0.045	0.035	0.066	0.073
HV 2339	1.142	12.101	12.084	12.078	12.113
		0.029	0.025	0.042	0.054
HV 2352	1.134	12.257	12.277	12.223	12.295
		0.082	0.034	0.066	0.090
HV 2352	1.134	12.393	12.341	12.298	12.337
		0.041	0.027	0.065	0.062
HV 2405	0.840	13.402	13.335	13.344	13.366
		0.047	0.036	0.073	0.101
HV 2405	0.840	13.250	13.296	13.109	13.171
		0.039	0.041	0.079	0.097
HV 2369	1.684	10.190	10.168	10.128	10.125
		0.039	0.036	0.035	0.049
HV 2369	1.684	10.133	10.169	10.109	10.083
		0.038	0.029	0.040	0.044

Table 1—Continued

Cepheid	log(P) (days)	3.6 μ m (mag)	4.5 μ m (mag)	5.8 μ m (mag)	8.0 μ m (mag)
HV 2432	1.038	12.459	12.438	12.530	12.414
		0.069	0.038	0.068	0.072
HV 2432	1.038	12.488	12.352	12.389	12.482
		0.045	0.043	0.059	0.083
HV 2527	1.112	12.669	12.610	12.562	12.530
		0.028	0.043	0.043	0.078
HV 2527	1.112	12.461	12.519	12.447	12.402
		0.036	0.033	0.071	0.066
HV 2538	1.142	12.219	12.245	12.153	12.083
		0.030	0.020	0.046	0.038
HV 2538	1.142	12.204	12.318	12.298	12.201
		0.034	0.028	0.033	0.053
HV 2549	1.209	11.738	11.759	11.738	11.718
		0.039	0.041	0.056	0.056
HV 2549	1.209	11.797	11.819	11.757	11.757
		0.030	0.028	0.052	0.046
HV 2579	1.128	12.104	12.121	12.078	12.075
		0.038	0.034	0.056	0.079
HV 2579	1.128	12.263	12.159	12.138	12.193
		0.051	0.031	0.058	0.051
HV 2580	1.228	11.721	11.821	11.763	11.707
		0.028	0.023	0.032	0.038
HV 2580	1.228	11.717	11.727	11.711	11.618
		0.038	0.034	0.054	0.048
HV 2733	0.941	12.856	12.820	12.848	12.812
		0.050	0.039	0.057	0.092
HV 2733	0.941	12.814	12.828	12.823	12.900
		0.036	0.033	0.058	0.065
HV 2749	1.364	11.720	11.768	11.690	11.543
		0.045	0.039	0.058	0.063

Table 1—Continued

Cepheid	log(P) (days)	3.6 μ m (mag)	4.5 μ m (mag)	5.8 μ m (mag)	8.0 μ m (mag)
HV 2749	1.364	11.763	11.645	11.616	11.598
		0.032	0.038	0.043	0.070
HV 2793	1.283	11.529	11.626	11.561	11.516
		0.031	0.044	0.053	0.055
HV 2793	1.283	11.699	11.784	11.621	11.644
		0.047	0.036	0.048	0.062
HV 2836	1.244	11.962	12.037	11.908	12.055
		0.031	0.034	0.061	0.053
HV 2836	1.244	11.953	12.109	11.973	11.943
		0.037	0.041	0.057	0.064
HV 2854	0.936	12.942	12.886	12.940	12.880
		0.029	0.029	0.048	0.067
HV 2854	0.936	12.779	12.743	12.684	12.798
		0.034	0.028	0.051	0.072
HV 5655	1.153	12.167	12.185	12.115	12.109
		0.050	0.040	0.054	0.065
HV 5655	1.153	12.120	12.150	12.149	12.110
		0.038	0.030	0.044	0.035
HV 6065	0.835	13.201	13.257	13.162	13.331
		0.036	0.040	0.076	0.105
HV 6065	0.835	13.414	13.365	13.310	13.285
		0.033	0.045	0.078	0.101
HV 6098	1.384	11.168	11.134	11.135	11.151
		0.027	0.027	0.028	0.032
HV 6098	1.384	11.189	11.126	11.086	11.089
		0.035	0.037	0.044	0.046
HV 8036	1.453	11.224	11.316	11.215	11.293
		0.041	0.043	0.043	0.053
HV 8036	1.453	11.360	11.466	11.385	11.287
		0.042	0.025	0.055	0.038

Table 1—Continued

Cepheid	log(P) (days)	3.6 μ m (mag)	4.5 μ m (mag)	5.8 μ m (mag)	8.0 μ m (mag)
HV 12471	1.200	12.044	12.129	12.030	12.007
		0.040	0.035	0.053	0.067
HV 12471	1.200	12.253	12.339	12.256	12.223
		0.034	0.041	0.060	0.057
HV 12505	1.158	12.416	12.453	12.533	12.460
		0.036	0.035	0.085	0.074
HV 12505	1.158	12.539	12.499	12.407	12.646
		0.044	0.036	0.061	0.085
HV 12656	1.127	12.339	12.299	12.289	12.301
		0.048	0.037	0.058	0.067
HV 12656	1.127	12.217	12.187	12.145	12.198
		0.056	0.041	0.054	0.078
HV 12700	0.911	12.910	12.908	12.989	12.899
		0.043	0.044	0.073	0.085
HV 12700	0.911	12.900	12.914	12.873	12.996
		0.035	0.030	0.066	0.071
HV 12724	1.138	12.326	12.365	12.338	12.316
		0.051	0.039	0.064	0.071
HV 12724	1.138	12.492	12.566	12.463	12.443
		0.046	0.040	0.073	0.063
HV 12815	1.416	11.063	11.125	11.059	11.007
		0.038	0.034	0.042	0.038
HV 12815	1.416	11.054	11.079	11.004	11.053
		0.030	0.024	0.029	0.033
HV 12816	0.973	12.897	12.844	12.901	12.956
		0.052	0.034	0.075	0.077
HV 12816	0.973	12.826	12.789	12.877	12.765
		0.035	0.036	0.061	0.085
HV 13048	0.836	13.084	13.088	13.067	13.054
		0.034	0.032	0.059	0.075

Table 1—Continued

Cepheid	log(P) (days)	3.6 μ m (mag)	4.5 μ m (mag)	5.8 μ m (mag)	8.0 μ m (mag)
HV 13048	0.836	13.217	13.197	13.060	13.058
		0.044	0.044	0.090	0.093
HV 2279	0.839	13.409	13.459	13.363	13.378
		0.047	0.047	0.100	0.146
HV 2279	0.839	13.346	13.472	13.463	13.186
		0.067	0.059	0.105	0.109
HV 886	1.380	11.488	11.550	11.481	11.450
		0.034	0.033	0.048	0.055
HV 886	1.380	11.667	11.232	11.552	11.585
		0.039	0.035	0.052	0.055
HV 12747	0.556	14.205	14.251	14.527	14.051
		0.044	0.058	0.174	0.185
HV 12747	0.556	14.224	14.193	14.135	13.999
		0.034	0.041	0.091	0.999